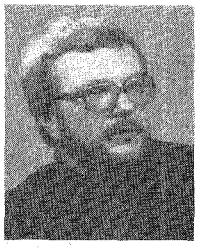

Klaus Schünemann (M'77) was born in Braunschweig, West Germany, on June 17, 1939. He received the master's degree in electrical engineering (Dipl.-Ing.) and his doctorate of engineering (Dr.-Ing.) from the Technische Universität Braunschweig, West Germany, in 1965 and 1970, respectively.

From 1965 to 1970 he was a Research Assistant at the Department of Electrical Engineering of the Technical University Braunschweig (Institut für Hochfrequenztechnik), where he was engaged in investigations on frequency multiplication and on diode modelling for switching applications. From 1970 to 1971 he worked for Valvo GmbH of Hamburg, West Germany, in the area of high-power, high-stable, solid-state oscillators. Since 1972, he has been back with the Institut für Hochfrequenztechnik (Electrical Engineering Department of the Technical University Braunschweig), where he has been involved with investigations on high-speed modulators for PCM communication systems and on amplification and noise in solid-state oscillators. He is now a Professor in the Electrical Engineering Department and his current research interests are primarily concerned with new technologies for microwave integrated circuits, such as fin-line and waveguide-below-cutoff techniques, and with transport phenomena in submicron structures.

Hybrid Fin-Line Matching Structures

HADIA EL HENNAWY, STUDENT MEMBER, IEEE, AND KLAUS SCHÜNEMANN, MEMBER, IEEE

Abstract—**Two transitions between unilateral and bilateral fin-line mounted back to back show unique features for impedance transformation. The series reactances of the equivalent T-circuit are theoretically shown to be capacitive. This is exploited by designing a broad-band switch with two p-i-n diodes. Its isolation is about 20 dB throughout the *Ka*-band.**

I. Introduction

THE BASIC building blocks of fin-line circuits are various discontinuities in the slot width. Impedance transformation is usually performed with either one or two steps in the slot width [1]. With two cascaded steps one can generate either a notch or a strip. Almost all known components are realized in this way. These structures can be analyzed by combining an eigenmode with a modal analysis [2]. The procedure has been carried through in [1]. We will apply this method here to new configurations.

The structures for impedance transformation to be described show both electrical and practical advantages over the known ones. Their slot patterns are sketched in Fig. 1. These structures consist of two cascaded transitions between unilateral and bilateral fin-lines of equal slot widths. The slot may be located either symmetrically or unsymmetrically with respect to the waveguide axis. A large range of impedances can be generated by varying two geometrical parameters: the common slot width $2s$ and the length $2l$ of the middle section. Such a line section can therefore be used in either of two ways: as an impedance transformer or as a semiconductor device mount. In the latter application, the circuit patterns show a practical advantage over conventional ones. While the circuit at the front side which contains the semiconductor devices is protected against damage, one can conveniently alter the transforming section on the back side of the substrate in order to optimize performance. In addition, there are, however, even electrical advantages over the usual notch and strip patterns, which will be derived in the following.

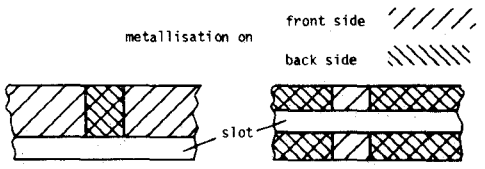

Fig. 1. Slot patterns of transitions between unilateral and bilateral fin-lines.

II. Modal Analysis

In order to analyze the structures shown in Fig. 1, one must know both the propagation constants and the field distributions of the hybrid eigenmodes of unilateral and bilateral fin-lines. The problem has been solved by a number of authors. We have adopted the spectral-domain technique presented, e.g., in [3] and modified it to determine the eigenmodes of both unilateral and bilateral fin-line in a unified form. The unilateral fin-line case is treated in Appendix I, while the results for the bilateral fin-line will be presented elsewhere [4]. The notation is the same for both cases. The key to an efficient eigenmode evaluation is a suitable choice of the system of basis functions into which the slot fields must be expanded. This has been discussed in [3]. We have used a fifth-order polynomial modified by a square-root term in order to take the edge condition correctly into account. Thus it was possible to calculate up to 30 eigenmodes with sufficient accuracy.

The modal analysis for computing the characteristics of an abrupt transition between a bilateral and a unilateral fin-line shall be briefly described (compare also to [5]). As

Manuscript received March 10, 1982; revised June 4, 1982.

K. Schünemann is with the Institut für Hochfrequenztechnik, Technische Universität Braunschweig, D-3300 Braunschweig, West Germany.

H. El Hennawy is with Ain Shams University, Cairo, Egypt.

0018-9480/82/1200-2132$00.75 ©1982 IEEE

shown in the slot patterns of Fig. 1, both the slot widths and the location of the slot above the broad wall of the waveguide are assumed to stay constant at both sides of the junction. The electric and magnetic fields of the ith eigenmode are written as

$$e_i(x,y,z) = a_i \bar{e}_i(x,y) e^{\pm \gamma_i z}$$
$$h_i(x,y,z) = a_i \bar{h}_i(x,y) e^{\pm \gamma_i z} \quad (1)$$

with $\bar{e}_i$ and $\bar{h}_i$ the transverse vector functions of the electric and magnetic field, respectively. Denoting the transverse field distribution of the left waveguide a at the junction ($z = 0$) by $\bar{E}_a$, $\bar{H}_a$, and expanding it in terms of the eigenmodes of that waveguide, reads

$$\bar{E}_a = (1+\rho) a_1 \bar{e}_{a1} + \sum_{i=2}^{\infty} a_i \bar{e}_{ai}$$
$$\bar{H}_a = (1-\rho) a_1 \bar{h}_{a1} - \sum_{i=2}^{\infty} a_i \bar{h}_{ai}. \quad (2)$$

Similarly, one writes for waveguide b

$$\bar{E}_b = \sum_{j=1}^{\infty} b_j \left(\bar{e}_{bj} + \sum_{k=1}^{\infty} s_{jk} \bar{e}_{bk} \right)$$
$$\bar{H}_b = \sum_{j=1}^{\infty} b_j \left(\bar{h}_{bj} - \sum_{k=1}^{\infty} s_{jk} \bar{h}_{bk} \right). \quad (3)$$

ρ means reflection coefficient of the incident mode ($i = 1$), s_{jk} are the scattering coefficients of the next discontinuity located at $z > 0$ in waveguide b.

In the following, we will address the so-called 'boundary reduction problem' (terminology taken from [2]), i.e., the cross section of waveguide a is larger than that of waveguide b. In our case, the former is a unilateral and the latter a bilateral fin-line. The boundary enlargement problem can be treated in the same way as described below, if the subscripts a and b in (2) and (3) are interchanged.

Equations (2) and (3) are used to formulate the boundary conditions at the junction, which are manipulated in the following way. The cross product of the electric field in (2) with $\bar{h}_{am}$ is taken and integrated over the cross section of waveguide a. For the unknown field on the left-hand side, $\bar{E}_b$ is inserted from (3). Similarly, the cross product of the magnetic field in (2) with $\bar{e}_{bn}$ is taken and integrated over the cross section of waveguide b. For the unknown field on the left-hand side, $\bar{H}_b$ is inserted from (3). One obtains

$$\begin{aligned}(1+\rho) a_1 \int_{(a)} \bar{e}_{a1} \times \bar{h}_{am} \cdot u_z \, dx\, dy \\ + \sum_{i=2}^{\infty} a_i \int_{(a)} \bar{e}_{ai} \times \bar{h}_{am} \cdot u_z \, dx\, dy \\ = \sum_{j=1}^{\infty} \left[b_j \left(\int_{(b)} \bar{e}_{bj} \times \bar{h}_{am} \cdot u_z \, dx\, dy \right.\right. \\ \left.\left. + \sum_{k=1}^{\infty} s_{jk} \int_{(b)} \bar{e}_{bk} \times \bar{h}_{am} \cdot u_z \, dx\, dy \right) \right] \quad (4a)\end{aligned}$$

$$\begin{aligned}(1-\rho) a_1 \int_{(b)} \bar{e}_{bn} \times \bar{h}_{a1} \cdot u_z \, dx\, dy \\ - \sum_{i=2}^{\infty} a_i \int_{(b)} \bar{e}_{bn} \times \bar{h}_{ai} \cdot u_z \, dx\, dy \\ = \sum_{j=1}^{\infty} \left[b_j \left(\int_{(b)} \bar{e}_{bn} \times \bar{h}_{bj} \cdot u_z \, dx\, dy \right.\right. \\ \left.\left. - \sum_{k=1}^{\infty} s_{jk} \int_{(b)} \bar{e}_{bn} \times \bar{h}_{bk} \cdot u_z \, dx\, dy \right) \right]. \quad (4b)\end{aligned}$$

u_z means unit vector in the z-direction. Because $\bar{E}_a$ exists on the common aperture only and vanishes elsewhere, the integrals on the right-hand side of (4a) must only be taken over the cross section of waveguide 'b'. These integrals can be solved once the eigenmodes have been formulated. The solutions are listed in Appendix II for the general case of a junction between two unilateral fin-lines. If a junction between a unilateral and a bilateral fin-line is to be treated, one must only omit some of the expansion coefficients. ($A_n^{(2)} = S_n^{(2)} = B_n^{(2)} = M_n^{(2)} = 0$ for an unsymmetrical mode in bilateral fin-line, $\bar{A}_n^{(2)} = \bar{S}_n^{(2)} = \bar{B}_n^{(2)} = \bar{M}_n^{(2)} = 0$ for a symmetrical mode.)

In order to solve (4) for the amplitudes of the excited modes, one must first determine the scattering coefficients s_{jk}. For a single transition, waveguide b may be assumed to be terminated in a matched load: $s_{jk} = 0$. For two transitions in cascade, we can take advantage of the symmetry of the structure with respect to the plane $z = l$. The equivalent circuit can then be found from both an even and an odd excitation of both ports, so that $s_{jk} = 0$ for $j \neq k$ and

$$s_{jj} = (1 - y_{bj})/(1 + y_{bj}) = \pm \exp(-2j\beta_{bj} l). \quad (5)$$

y_{bj} is the normalized input admittance of the jth mode in waveguide b measured at $z = 0$, and β_{bj} means propagation constant of this mode.

We are now in a position to solve the system of equations (4). It is convenient to normalize the wave amplitudes on a_1. Setting

$$a_i' = a_i/a_1, \quad b_j' = b_j/a_1, \quad I'_{ambj} = I_{ambj}/(F_{am} F_{bj}) \quad (6)$$

with the I's and F's taken from Appendix II we obtain for the case that the exciting wave a_1 impinges on waveguide b from waveguide a

$$\rho I'_{a1bn} + \sum_{i=2}^{L} a_i' I'_{aibn} - \sum_{j=1}^{L} b_j' (1 + s_{jj}) I'_{bjbn} = -I'_{a1bn}$$
$$\rho I'_{ama1} + \sum_{i=2}^{L} a_i' I'_{amai} + \sum_{j=1}^{L} b_j' (1 - s_{jj}) I'_{ambj} = I'_{ama1}. \quad (7)$$

These relations are valid for the boundary enlargement problem, i.e., that waveguide a is a bilateral and waveguide b a unilateral fin-line. If a wave a_1 impinges from b on a,

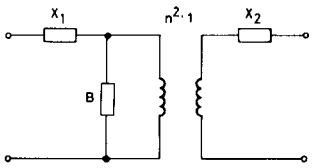

Fig. 2. Equivalent circuit of a single transition (port 1 = bilateral, port 2 = unilateral fin-line).

one obtains for the boundary reduction problem

$$\rho I'_{b1bm} + \sum_{i=2}^{L} a'_i I'_{bibm} - \sum_{j=1}^{L} b'_j (1+s_{jj}) I'_{ajbm} = -I'_{b1bm}$$

$$\rho I'_{anb1} + \sum_{i=2}^{L} a'_i I'_{anbi} + \sum_{j=1}^{L} b'_j (1-s_{jj}) I'_{anaj} = I'_{anb1}. \quad (8)$$

The infinite series are truncated at $i = j = L$, thus taking L modes in each waveguide into account. Then (7) or (8) generate $2L$ linear equations for $1+(L-1)+L$ unknowns.

A single transition from unilateral to bilateral fin-line is characterized by an equivalent circuit shown in Fig. 2 whose elements can be computed from the input admittances at both ports. Two cascaded transitions are represented by a T-equivalent circuit with series reactances X_{sc} and shunt reactances $(X_{oc} - X_{sc})/2$. (Subscripts *sc* denote a short circuit, subscripts *oc* an open circuit at the symmetry plane $z = l$.)

III. Performance of Transitions

The modal analysis has been applied to a single transition between unilateral and bilateral fin-line and to the cascaded transitions sketched in Fig. 1. Some results for the elements of the equivalent circuit of a single transition (Fig. 2) are shown in Fig. 3. (The turns ratio of the ideal impedance transformer has been omitted because it is very close to unity.) The general shape of the three remaining elements (note that subscript 1 refers to the bilateral fin-line port) can be explained by assuming an electric field directed perpendicularly through the dielectric substrate from front to back fin of the bilateral fin-line. This field can of course exist only in the immediate vicinity of the transition between the two fin-lines. For larger slot widths ($2s$), the substrate thickness ($2d$) is much smaller than ($2s$). Hence, a capacitive series reactance X_1 appears in the equivalent circuit. The shunt susceptance B is small because the slot width approaches the waveguide height ($2b$). The electric field concentration in the slot increases with decreasing ($2s$). Hence, B must increase monotonically and X_1 must increase, too. Finally, X_1 becomes inductive because of an increasing magnetic field concentration which is due to a surface current filament on the transversely oriented fin edge of the bilateral fin-line.

The most important result is that there may exist a capacitive series reactance. It will be shown below that the potentials for impedance transformation in fin-lines will be largely amplified by this.

The equivalent circuit elements of two cascaded transitions are shown in Fig. 4 versus the length of the middle

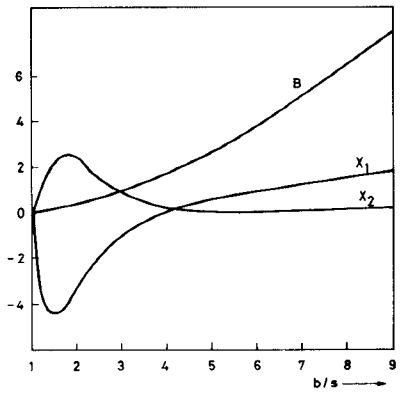

Fig. 3. Elements of the equivalent circuit of a single transition (Fig. 2) versus slot width ($2s$) normalized against waveguide height ($2b$). The elements are normalized against the wave impedance of the adjacent port. (Frequency 30 GHz, WR-28 waveguide with $2a = 7.112$ mm, $2b = 3.556$ mm, symmetrically located slot of width $2s$, RT-duroid 5880 substrate of thickness $2d = 0.254$ mm and relative dielectric constant $\epsilon_r = 2.22$.)

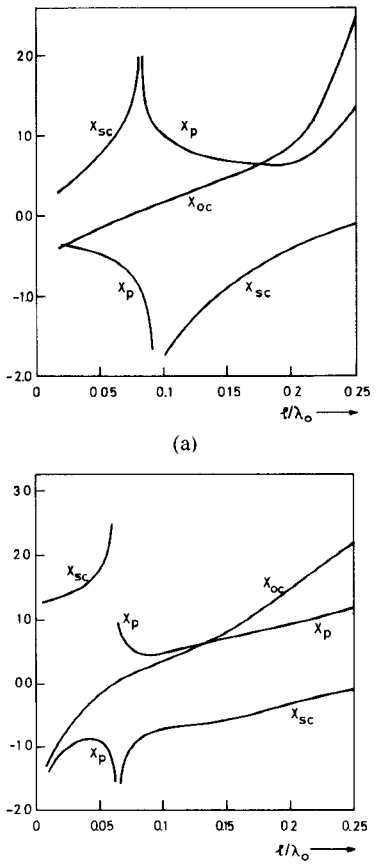

Fig. 4 (a) Elements of the equivalent T-circuit of a section of bilateral fin-line (length $2l$) embedded into a unilateral fin-line. The elements are normalized against the wave impedance of the unilateral fin-line. λ_0 means free-space wavelength. (Parameters as in Fig. 3 with $2s = 0.4$ mm.) (b) Elements of the equivalent T-circuit of a section of unilateral fin-line embedded into a bilateral fin-line. (Normalization against bilateral fin-line impedance; parameters as in Fig. 4(a).)

section. The slot width is relatively small: $s = 0.2$ mm. The shape of the curves can be explained by cascading the equivalent circuits of two single transitions. (They have, however, been computed by taking higher order mode

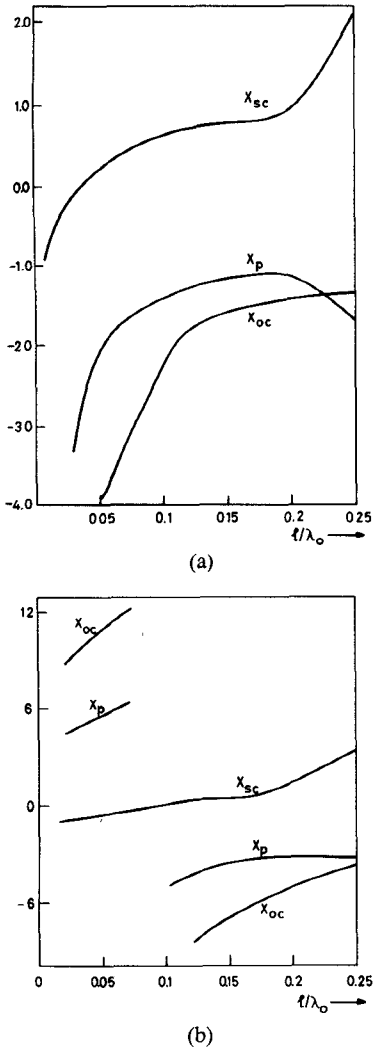

Fig. 5. (a) T-circuit elements as in Fig. 4(a) with $2s = 1.0$ mm. (b) T-circuit elements as in Fig. 4(b) with $2s = 1.0$ mm.

coupling into account.) A significant feature is the parallel resonant behavior of the series reactance for small lengths l, which can be explained if the two cascaded transitions are separately regarded (i.e., if higher order mode coupling between them is neglected). The series reactance is calculated for odd excitation so that one port of the equivalent circuit of Fig. 2 is terminated in a short-circuited transmission line of length l. Hence, the parallel resonant behavior of X_{sc} is due to B resonating with X_1 and the input reactance of the transmission line.

The series reactance is capacitive for larger lengths l. This is of great importance for circuit design because there is no other discontinuity known showing a capacitive series reactance. (Both notch and strip show an inductive series reactance [1].) This unique feature of a double transition between unilateral and bilateral fin-line offers an interesting alternative in the design of p-i-n-diode switches as will be illustrated below. It can, however, be observed only for small slot widths. The series reactance is inductive, if s exceeds a certain limit. This is illustrated by the results shown in Fig. 5. Instead of a parallel resonance, X_{sc} now shows series-resonant behavior. This can again be explained by means of the simplified equivalent circuit. The shunt susceptance B of a single transition can now be neglected (compare with Fig. 3!), so that X_1 is in series with the short-circuited transmission line of length l (odd excitation). Hence, X_{sc} models a series circuit. The shunt element X_p is, however, always capacitive.

IV. Design of a Broad-Band Switch

The unique characteristic of a section of bilateral fin-line embedded into a unilateral fin-line shall now be utilized to design a broad-band switch with two p-i-n diodes. The diodes are usually bonded across a narrow fin-line slot [7] within a distance of about a quarter of a wavelength in order to obtain broad-band performance. Then one needs three diodes in order to guarantee 20-dB isolation over a waveguide band [7]. Using the matching structures discussed above will, however, reduce the number of diodes for nearly the same performance to 2.

A p-i-n diode can approximately be characterized by its package inductance in on-state and by its i-layer capacitance shunted by the package capacitance in off-state. The on-state of the diode normally corresponds to the isolation state of the switch (diode mounted in shunt to the transmission line). Hence, the package inductance must be carefully tuned in order to enhance isolation. Guidelines for designing a broad-band switch with two p-i-n diodes in shunt are derived in detail in [8]. Both diodes should be about a quarter of a wavelength spaced. Broad-band performance demands to compensate for the package inductances at two different frequencies f_a and f_b, which are related to the upper and lower corner frequencies f_1, f_2 via [8]

$$f_{a,b} = \left[\left(\frac{f_1+f_2}{2}\right)^2 \pm \sqrt{\left(\frac{f_1+f_2}{2}\right)^4 - (f_1 f_2)^2}\right]^{1/2}. \quad (9)$$

The two sections of bilateral fin-line which are used to tune the diodes in their on-state must, hence, show different lengths. The slot pattern of the switch and its equivalent circuit are sketched in Fig. 6. One recognizes that a capacitive series reactance X_{sc} is necessary in order to fulfill the said tuning condition. (Hence, neither a notch nor a strip can be used instead.) Following the design rules given in [8], the equivalent circuit should present a bandpass characteristic with, e.g., a maximally flat response in the transmission state. This is achieved for $X = 2B$ with X and B defined in Fig. 6. Thus, the length of the unilateral fin-line between both diode mounts is fixed. In the isolation state, series resonance is claimed at f_a and f_b, respectively. This determines the lengths of the two mounting sections. The common slot width should correspond to the physical size of the diode package.

We have realized a Ka-band switch with two p-i-n diodes 4701 (Microwave Associates). The slot width has been chosen to $2s = 0.4$ mm. Measuring the diode impedance in a bilateral fin-line of equal slot width yields the input data of the design procedure referred to the diode plane.

$Z_{on} = 0.19 + j0.15$, $Z_{off} = -j6.53$ at $f_b = 28$ GHz, $Z_{on} =$

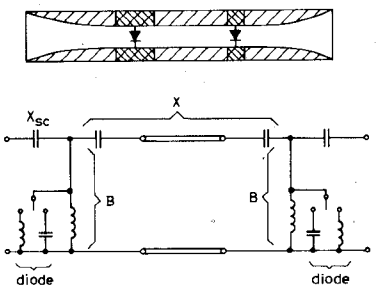

Fig. 6. Slot pattern and equivalent circuit of a switch with two p-i-n diodes 7401 (Microwave Associates).

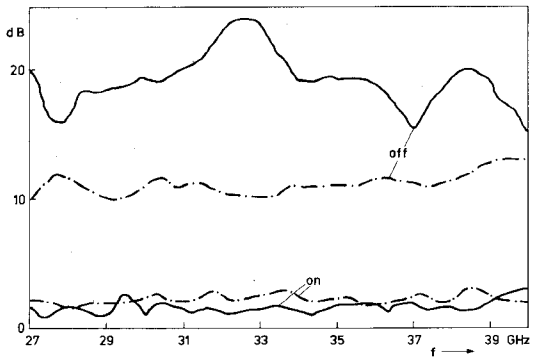

Fig. 7. Performance of the switch from Fig. 6. Solid lines: hybrid fin-line circuit. Dashed-dotted lines: all unilateral fin-line, diodes quarter of a wavelength apart.

$0.31 + j0.89$, $Z_{off} = 0.45 - j1.02$ at $f_a = 38$ GHz. Neglecting the real parts, the length of each section has to tune out Z_{on}. One recognizes from Fig. 4(a) that the shunt reactance X_p of the unloaded section shows a broad minimum versus the length l. It is hence reasonable to start with a guessed $X_p = 0.7$ taken from the minimum range. The total shunt reactance of the loaded section being known, the condition for series resonance can be evaluated for X_{sc}. This fixes l so that the choice for X_p can be checked. Repeating this cycle one obtains $l_1 = 2.2$ mm; $l_2 = 1.6$ mm. To simplify the following calculations, the frequency dependence of the equivalent circuit elements will be neglected. They are calculated at the center frequency 32 GHz: $jX_{sc1} = -0.25$, $jX_{p1} = 0.8$, $jX_{sc2} = -0.784$, $jX_{p2} = 0.75$. Then the condition for maximally flat response in the transmission state can be evaluated yielding a net length for the unilateral fin-line between the mounting sections of 4.0 mm.

The performance of the realized switch is shown in Fig. 7. These results have been obtained without any modification of the calculated slot pattern and without any adjustment. The isolation is much better than for a simple switch with the two diodes mounted a quarter of a wavelength apart in a unilateral fin-line. The isolation is about 19 dB, the insertion loss less than 2 dB. No efforts have, however, been undertaken in order to minimize the dissipative losses. Hence, it can be concluded that hybrid fin-line circuits offer new potentials to circuit design.

V. Conclusions

Using a modal analysis, cascaded transitions between unilateral and bilateral fin-lines have been investigated. These structures show a unique feature: a capactive instead of an inductive series reactance of the equivalent T-circuit. This cannot be obtained with any other known discontinuity in fin-lines. It is illustrated that this new degree of freedom can advantageously be utilized in the design of broad-band switches. The isolation obtained with two p-i-n diodes is nearly the same as has as yet been achieved with three diodes. Moreover, there are practical advantages in that a semiconductor device mount can easily be modified without affecting the device itself. Hence, the combination of unilateral and bilateral fin-lines seems to be an interesting alternative to conventional notch and strip patterns. Other applications like filters and FET mounts are also imaginable.

Appendix I

The unified calculation of the hybrid eigenmodes will only briefly be sketched because it has recently been described elsewhere [4] for the bilateral fin-line. Hence, we will complete those derivations by treating the unilateral fin-line case. The notation is the same as in [4].

The fin-line cross section is shown in Fig. 8. The slot width is $2s = d_1 - d_2$. Because of symmetry an electric wall (e.w.) may be assumed on the x-axis. The fields are derived from the E_x- and H_x-components which must satisfy the Helmholtz equation.

The transverse electric field components are written

$$E_{ti}^{(1)} = \sum_{n=1}^{\infty} A_n^{(1)} \cos \bar{\alpha}_n (x-a) \sin \alpha_n y \cdot u_x + \sum_{n=0}^{\infty} S_n^{(1)} \sin \bar{\alpha}_n (x-a) \cos \alpha_n y \cdot u_y$$

$$E_{ti}^{(3)} = \sum_{n=1}^{\infty} A_n^{(3)} \cos \bar{\alpha}_n (x+a) \sin \alpha_n y \cdot u_x + \sum_{n=0}^{\infty} S_n^{(3)} \sin \bar{\alpha}_n (x+a) \cos \alpha_n y \cdot u_y$$

$$E_{ti}^{(2)} = \sum_{n=1}^{\infty} \left(A_n^{(2)} \sin \tilde{\alpha}_n x \sin \alpha_n y + \bar{A}_n^{(2)} \cos \tilde{\alpha}_n x \sin \alpha_n y \right) \cdot u_x + \sum_{n=0}^{\infty} \left(S_n^{(2)} \cos \tilde{\alpha}_n x \cos \alpha_n y + \bar{S}_n^{(2)} \sin \tilde{\alpha}_n x \cos \alpha_n y \right) \cdot u_y \tag{A1}$$

with

$$\bar{\alpha}_n = \sqrt{k_0^2 - \beta^2 - \alpha_n^2}, \qquad \tilde{\alpha}_n = \sqrt{\epsilon_r k_0^2 - \beta^2 - \alpha_n^2}, \quad \alpha_n = n\pi/b. \tag{A2}$$

k_0 means free-space wavenumber, β propagation constant. u_x and u_y are unit vectors in the x- and y-directions, respectively. For the magnetic field components, one has similarly

$$H_{ti}^{(1)} = \sum_{n=0}^{\infty} \left(B_n^{(1)} \sin \bar{\alpha}_n (x-a) \cos \alpha_n y \right) \cdot u_x + \sum_{n=1}^{\infty} \left(M_n^{(1)} \cos \bar{\alpha}_n (x-a) \sin \alpha_n y \right) \cdot u_y$$

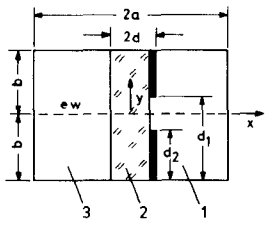

Fig. 8. Cross section of a unilateral fin-line (e.w. means electric wall).

$$H_{ti}^{(3)} = \sum_{n=0}^{\infty} \left(B_n^{(3)} \sin \bar{\alpha}_n (x+a) \cos \alpha_n y \right) \cdot u_x + \sum_{n=1}^{\infty} \left(M_n^{(3)} \cos \bar{\alpha}_n (x+a) \sin \alpha_n y \right) \cdot u_y$$

$$H_{ti}^{(2)} = \sum_{n=0}^{\infty} \left(B_n^{(2)} \cos \tilde{\alpha}_n x \cos \alpha_n y + \bar{B}_n^{(2)} \sin \tilde{\alpha}_n x \cos \alpha_n y \right) \cdot u_x + \sum_{n=1}^{\infty} \left(M_n^{(2)} \sin \tilde{\alpha}_n x \sin \alpha_n y + \bar{M}_n^{(2)} \cos \tilde{\alpha}_n x \sin \alpha_n y \right) \cdot u_y . \tag{A3}$$

The expansion coefficients are related via [4, eqs. (B4)]. In addition,

$$\begin{aligned} \bar{S}_n^{(2)} &= \left(- \bar{A}_n^{(2)} \alpha_n \tilde{\alpha}_n - jk_0 \beta \bar{B}_n^{(2)} \right) / \left(\beta^2 + \alpha_n^2 \right) \\ S_n^{(3)} &= \left(- A_n^{(3)} \alpha_n \bar{\alpha}_n - jk_0 \beta B_n^{(3)} \right) / \left(\beta^2 + \alpha_n^2 \right) \\ \bar{M}_n^{(2)} &= \left(- \bar{B}_n^{(2)} \alpha_n \tilde{\alpha}_n - jk_0 \beta \epsilon_r \bar{A}_n^{(2)} \right) / \left(\beta^2 + \alpha_n^2 \right) \\ M_n^{(3)} &= \left(- B_n^{(3)} \alpha_n \bar{\alpha}_n - jk_0 \beta A_n^{(3)} \right) / \left(\beta^2 + \alpha_n^2 \right). \end{aligned} \tag{A4}$$

Matching the tangential field components at the various interfaces yields equations (B5) of [4] and

$$A_n^{(2)} = A_n^{(3)} \left(\frac{-\bar{\alpha}_n}{\tilde{\alpha}_n} \cos \tilde{\alpha}_n d \sin \bar{\alpha}_n (a-d) - \frac{\sin \tilde{\alpha}_n d \cos \bar{\alpha}_n (a-d)}{\epsilon_r} \right)$$

$$\bar{A}_n^{(2)} = A_n^{(3)} \left(\frac{\cos \tilde{\alpha}_n d \cos \bar{\alpha}_n (a-d)}{\epsilon_r} - \frac{\bar{\alpha}_n}{\tilde{\alpha}_n} \sin \tilde{\alpha}_n d \sin \bar{\alpha}_n (a-d) \right)$$

$$B_n^{(2)} = B_n^{(3)} \left(\sin \bar{\alpha}_n (a-d) \cos \tilde{\alpha}_n d + \frac{\bar{\alpha}_n}{\tilde{\alpha}_n} \cos \bar{\alpha}_n (a-d) \sin \tilde{\alpha}_n d \right)$$

$$\bar{B}_n^{(2)} = B_n^{(3)} \left(\frac{\bar{\alpha}_n}{\tilde{\alpha}_n} \cos \tilde{\alpha}_n d \cos \bar{\alpha}_n (a-d) - \sin \bar{\alpha}_n (a-d) \sin \tilde{\alpha}_n d \right)$$

$$A_n^{(3)} = - A_n^{(1)} \sin \bar{\alpha}_n (a-d) \Big/ \left(\cos 2\tilde{\alpha}_n d \sin \bar{\alpha}_n (a-d) + \frac{\tilde{\alpha}_n}{\epsilon_r \bar{\alpha}_n} \sin 2\tilde{\alpha}_n d \cos \bar{\alpha}_n (a-d) \right)$$

$$B_n^{(3)} = - B_n^{(1)} \sin \bar{\alpha}_n (a-d) \Big/ \left(\cos 2\tilde{\alpha}_n d \sin \bar{\alpha}_n (a-d) + \frac{\bar{\alpha}_n}{\tilde{\alpha}_n} \sin 2\tilde{\alpha}_n d \cos \bar{\alpha}_n (a-d) \right). \tag{A5}$$

The remaining expansion coefficients are expressed in terms of the slot field components $E_y(y)$ and $E_z(y)$ after Fourier transforming all field components and boundary conditions with respect to y. The results are given in [4, eqs. (B6) and (B7)]. The problem of finding the EM field distribution has thus been reduced to determining the slot fields. This is solved by applying Ritz–Galerkin's method. The procedure has been carried through in [3] and in [4, appendix B] to which the reader is referred.

Appendix II

The integrals appearing in (4) are solved by inserting the transverse field configurations given in Appendix I. One obtains

$$\begin{aligned} I_{aibj} &= \int_{(a,b)} \bar{e}_{ai} \times \bar{h}_{bj} \cdot u_z \, dx \, dy \\ &= \frac{b}{2} \sum_{n=0}^{\infty} \Bigg\{ \left[\delta_n \left(A_{na}^{(1)} M_{nb}^{(1)} + A_{na}^{(3)} M_{nb}^{(3)} \right) - \eta_1 \epsilon_n \left(B_{nb}^{(1)} S_{na}^{(1)} - B_{nb}^{(3)} S_{na}^{(3)} \right) \right] \cdot \frac{\sin (\bar{\alpha}_{nai} - \bar{\alpha}_{nbj})(a-d)}{2(\bar{\alpha}_{nai} - \bar{\alpha}_{nbj})} \\ &\quad + \left[\delta_n \left(A_{na}^{(1)} M_{nb}^{(1)} + A_{na}^{(3)} M_{nb}^{(3)} \right) + \eta_1 \epsilon_n \left(B_{nb}^{(1)} S_{na}^{(1)} + B_{nb}^{(3)} S_{na}^{(3)} \right) \right] \cdot \frac{\sin (\bar{\alpha}_{nai} + \bar{\alpha}_{nbj})(a-d)}{2(\bar{\alpha}_{nai} + \bar{\alpha}_{nbj})} \\ &\quad + \left[\eta_2 \delta_n \left(A_{na}^{(2)} M_{nb}^{(2)} + \bar{A}_{na}^{(2)} \bar{M}_{nb}^{(2)} \right) + \epsilon_n \left(B_{nb}^{(2)} S_{na}^{(2)} + \bar{B}_{nb}^{(2)} \bar{S}_{na}^{(2)} \right) \right] \frac{\sin (\tilde{\alpha}_{nai} - \tilde{\alpha}_{nbj}) d}{(\tilde{\alpha}_{nai} - \tilde{\alpha}_{nbj})} \\ &\quad - \left[\eta_2 \delta_n \left(A_{na}^{(2)} M_{nb}^{(2)} - \bar{a}_{na}^{(2)} \bar{M}_{nb}^{(2)} \right) + \epsilon_n \left(B_{nb}^{(2)} S_{na}^{(2)} - \bar{B}_{nb}^{(2)} \bar{S}_{na}^{(2)} \right) \right] \cdot \frac{\sin (\tilde{\alpha}_{nai} + \tilde{\alpha}_{nbj}) d}{(\tilde{\alpha}_{nai} + \tilde{\alpha}_{nbj})} \Bigg\} \end{aligned} \tag{A6}$$

$$\eta_1 = \begin{cases} 1, & \text{for } \bar{\alpha}_{nbj} \text{ real} \\ -1, & \text{for } \bar{\alpha}_{nbj} \text{ imaginary,} \end{cases} \qquad \delta_n = \begin{cases} 0, & \text{for } n = 0 \\ 1, & \text{for } n \neq 0 \end{cases}$$

$$\eta_2 = \begin{cases} 1, & \text{for } \tilde{\alpha}_{nbj} \text{ real} \\ -1, & \text{for } \tilde{\alpha}_{nbj} \text{ imaginary,} \end{cases} \qquad \epsilon_n \begin{cases} 1, & \text{for } n \neq 0 \\ 2, & \text{for } n = 0 \end{cases}. \tag{A7}$$

Also

$$F_{ai}^2 = \int_{(a,b)} \bar{e}_{ai}\, \bar{e}_{ai}^*\, dx\, dy$$

$$= \frac{b}{2} \sum_{n=0}^{\infty} \Bigg\{ \Big[\delta_n \big(|A_n^{(1)}|^2 + |A_n^{(3)}|^2 \big) + \eta_1 \epsilon_n \big(|S_n^{(1)}|^2 + |S_n^{(3)}|^2 \big) \Big] \cdot \frac{a-d}{2} + \Big[\delta_n \big(|A_n^{(1)}|^2 + |A_n^{(3)}|^2 \big) - \eta_1 \epsilon_n \cdot \big(|S_n^{(1)}|^2 + |S_n^{(3)}|^2 \big) \Big] \cdot \frac{\sin 2\bar{\alpha}_n (a-d)}{4\bar{\alpha}_n}$$

$$+ \Big[\eta_2 \delta_n \big(|A_n^{(2)}|^2 + |\bar{A}_n^{(2)}|^2 \big) + \epsilon_n \big(|S_n^{(2)}|^2 + |\bar{S}_n^{(2)}|^2 \big) \Big] \cdot d - \Big[\eta_2 \delta_n \big(|A_n^{(2)}|^2 - |\bar{A}_n^{(2)}|^2 \big) - \epsilon_n \big(|S_n^{(2)}|^2 - |\bar{S}_n^{(2)}|^2 \big) \Big] \cdot \frac{\sin 2\tilde{\alpha}_n d}{2\tilde{\alpha}_n} \Bigg\} \tag{A8}$$

$$I_{aiai} = \int_{(a,b)} \bar{e}_{ai} \times \bar{h}_{ai} \cdot u_z\, dx\, dy$$

$$= \frac{b}{2} \sum_{n=0}^{\infty} \Bigg\{ \Big[\delta_n \big(A_{na}^{(1)} M_{na}^{(1)} + A_{na}^{(3)} M_{na}^{(3)} \big) - \eta_1 \epsilon_n \big(S_{na}^{(1)} B_{na}^{(1)} + S_{na}^{(3)} B_{na}^{(3)} \big) \Big] \cdot \frac{a-d}{2} + \Big[\delta_n \big(A_{na}^{(1)} M_{na}^{(1)} + A_{na}^{(3)} M_{na}^{(3)} \big) + \eta_1 \epsilon_n \big(B_{na}^{(1)} S_{na}^{(1)} + B_{na}^{(3)} S_{na}^{(3)} \big) \Big] \cdot \frac{\sin 2\bar{\alpha}_n (a-d)}{4\bar{\alpha}_n}$$

$$+ \Big[\eta_2 \delta_n \big(A_{na}^{(2)} M_{na}^{(2)} + \bar{A}_{na}^{(2)} \bar{M}_{na}^{(2)} \big) - \epsilon_n \big(B_{na}^{(2)} S_{na}^{(2)} + \bar{B}_{na}^{(2)} \bar{S}_{na}^{(2)} \big) \Big] \cdot d - \Big[\eta_2 \delta_n \big(A_{na}^{(2)} M_{na}^{(2)} - \bar{A}_{na}^{(2)} \bar{M}_{na}^{(2)} \big) + \epsilon_n \big(B_{na}^{(2)} S_{na}^{(2)} - \bar{B}_{na}^{(2)} \bar{S}_{na}^{(2)} \big) \Big] \cdot \frac{\sin 2\tilde{\alpha}_n d}{2\tilde{\alpha}_n} \Bigg\} \tag{A9}$$

$$I_{aiaj} = \int_{(a,b)} \bar{e}_{ai} \times \bar{h}_{aj} \cdot u_z\, dx\, dy$$

$$= \frac{b}{2} \sum_{n=0}^{\infty} \Bigg\{ \Big[\delta_n \big(A_{nai}^{(1)} M_{naj}^{(1)} + A_{naj}^{(3)} M_{naj}^{(3)} \big) - \epsilon_n \big(B_{naj}^{(1)} S_{nai}^{(1)} + B_{naj}^{(3)} S_{nai}^{(3)} \big) \Big] \cdot \frac{\sin(\bar{\alpha}_{ni} - \bar{\alpha}_{nj})(a-d)}{2(\bar{\alpha}_{ni} - \bar{\alpha}_{nj})} + \Big[\delta_n \big(A_{nai}^{(1)} M_{naj}^{(1)} + A_{nai}^{(3)} M_{naj}^{(3)} \big) + \epsilon_n \big(B_{naj}^{(1)} S_{nai}^{(1)} + B_{naj}^{(3)} S_{nai}^{(3)} \big) \Big] \cdot \frac{\sin(\bar{\alpha}_{ni} + \bar{\alpha}_{nj})(a-d)}{2(\bar{\alpha}_{ni} + \bar{\alpha}_{nj})}$$

$$+ \Big[\delta_n \big(A_{nai}^{(2)} M_{naj}^{(2)} + \bar{A}_{nai}^{(2)} \bar{M}_{naj}^{(2)} \big) - \epsilon_n \big(B_{naj}^{(2)} S_{nai}^{(2)} + \bar{B}_{naj}^{(2)} \bar{S}_{nai}^{(2)} \big) \Big] \cdot \frac{\sin(\tilde{\alpha}_{ni} - \tilde{\alpha}_{nj})\, d}{(\tilde{\alpha}_{ni} - \tilde{\alpha}_{nj})} - \Big[\delta_n \big(A_{nai}^{(2)} M_{naj}^{(2)} - \bar{A}_{nai}^{(2)} \bar{M}_{naj}^{(2)} \big) + \epsilon_n \big(B_{naj}^{(2)} S_{nai}^{(2)} - \bar{B}_{naj}^{(2)} \bar{S}_{nai}^{(2)} \big) \Big] \cdot \frac{\sin(\tilde{\alpha}_{ni} + \tilde{\alpha}_{nj})\, d}{(\tilde{\alpha}_{ni} + \tilde{\alpha}_{nj})} \Bigg\}. \tag{A10}$$

Some of the subscripts in (A6)–(A10) have been omitted if they were not necessary for a unique characterization. The integral F_{ai}^2 is used later for normalization. The infinite series in the above formulas should be truncated at $N = Mb/s$ in order to take the edge condition accurately into account [6]. M is the number of components used in the system of basis functions. We have chosen $M = 4$.

Acknowledgment

The authors are indebted to the Deutsche Forschungsgemeinschaft for financial support.

References

[1] H. El Hennawy and K. Schünemann, "Analysis of fin-line discontinuities," in *Proc. 9th Euro. Microwave Conf.*, (Brighton), 1979, pp. 448–452.

[2] A. Wexler, "Solution of waveguide discontinuities by modal analysis," *IEEE Trans. Microwave Theory Tech.*, vol. MTT-15, pp. 508–517, 1967.

[3] L. P. Schmidt and T. Itoh, "Spectral domain analysis of dominant and higher order modes in fin-lines," *IEEE Trans. Microwave Theory Tech.*, vol. MTT-28, pp. 981–985, 1980.

[4] H. El Hennawy and K. Schünemann, "Impedance transformation in fin-lines," *Proc. Inst. Elec. Eng.*, part H: MOA, 1982.

[5] R. F. Harrington, *Time-Harmonic Electromagnetic Fields*. New York: McGraw-Hill, 1961.

[6] R. Mittra, T. Itoh, and T. Li, "Analytical and numerical studies of the relative convergence phenomenon arising in the solution of an integral equation by the moment method," *IEEE Trans. Microwave Theory Tech.*, vol. MTT-20, pp. 96–104, 1972.

[7] H. Meinel, B. Adelseck, and H. Callsen, "A survey of planar integrated millimeter-wave components," in *Military Microwaves Symp. Dig.*, (London, England), 1980, pp. 82–87.

[8] J. L. White, *Semiconductor Control*. New York: Artech, sec. 4, 1977.

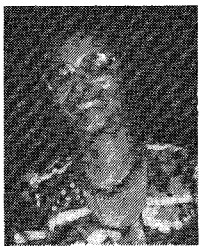

Hadia El Hennawy (S'74) was born in Tanta, Egypt, on November 25, 1949. She received the master's degree in electrical engineering (M.Sc.) from Ain Shams University, Cairo, and the doctorate of engineering (Dr.-Ing.) from the Technische Universität Braunschweig, West Germany, in 1976 and 1982, respectively.

From 1972–1978 she was a Research Assistant at the Department of Electronics and Computer Engineering, Ain Shams University, Cairo, where she was engaged in studies on the Gunn effect and on Gunn oscillators. From 1978–1982 she joined the Institut für Hochfrequenztechnik of the Technical University in Braunschweig, West Germany, where she has been involved with investigations on computer-aided design of integrated fin-line circuits. She is now back with the Ain Shams University in Cairo. Her current research interests are primarily concerned with integrated circuit techniques.

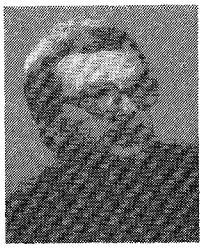

Klaus Schünemann (M'77) was born in Braunschweig, West Germany, on June 17, 1939. He received the master's degree in electrical engineering (Dipl.-Ing.) and his doctorate of engineering (Dr.-Ing.) from the Technische Universität Braunschweig, West Germany, in 1965 and 1970, respectively.

From 1965 to 1970 he was a Research Assistant at the Department of Electrical Engineering of the Technical University Braunschweig (Institut für Hochfrequenztechnik), where he was engaged in investigations on frequency multiplication and on diode modelling for switching applications. From 1970 to 1971 he worked for Valvo GmbH of Hamburg, West Germany, in the area of high-power, high-stable, solid-state oscillators. Since 1972, he has been back with the Institut

für Hochfrequenztechnik (Electrical Engineering Department of the Technical University Braunschweig), where he has been involved with investigations on high-speed modulators for PCM communication systems and on amplification and noise in solid-state oscillators. He is now a Professor in the Electrical Engineering Department and his current research interests are primarily concerned with new technologies for microwave integrated circuits, such as fin-line and waveguide-below-cutoff techniques, and with transport phenomena in submicron structures.

Modal Solutions of Active Dielectric Waveguides by Approximate Methods

A. LINZ, MEMBER, IEEE, AND J. K. BUTLER, SENIOR MEMBER

Abstract—**Approximate methods are used to obtain the modal properties of stripe-contact semiconductor injection lasers using a planar three-layer waveguide model. The central active layer has a dielectric constant that varies smoothly along the direction parallel to the heterojunction boundaries. The complex dielectric constant under the stripe contact is dependent on the gain and approaches a constant value at large lateral distances. The two methods are compared in terms of their modal propagation constants. An application of the effective index method facilitates a physical understanding of dielectric waveguide modes as well as providing an efficient calculation procedure.**

I. INTRODUCTION

ANALYSIS OF mode propagation in dielectric waveguides with a spatially varying refractive index has been the subject of several papers [1]–[3]. Typically, the variation of the dielectric constant with distance has been approximated with a parabolic profile [1], [2] or a function of the form $\kappa = -\kappa_0 + \kappa_3 \tanh^2(x/x_0)$ [3]. Both approximations have the disadvantage that the value of κ goes to infinity at large distances from the point $x = 0$, which corresponds to the axis of lateral symmetry of the structure. In the case of a semiconductor laser, this corresponds to the region below the center of the contact stripe. Another approximation that eliminates this disadvantage is the use of a function of the form [4]

$$\kappa = \kappa_S + \Delta\kappa/\cosh^2(x/x_0) \tag{1}$$

to describe the variation of κ. This is in closer correspondence with the physical situation, since κ now acquires the value κ_S for $x \gg x_0$. Even if this particular form of variation of κ does not describe the actual variation very closely, it retains the most important features, and leads to equations with known solutions. The disadvantage in this case is the fact that the field solutions consist of a finite (possibly empty) set of confined trapped modes, an infinite set of discrete, diverging "leaky" modes, and a continuum of solutions that will be designated as "radiation" modes, as opposed to an infinite set of discrete trapped modes only, as in the parabolic and $\tanh^2(x/x_0)$ profiles. Mode analysis is a two-dimensional problem, since the refractive index varies in both lateral (x) and transverse (y) directions. Therefore, numerical or approximate methods need to be applied. The most popular and effective approximation method is the "effective-index" solution, whereby the two-dimensional problem is reduced to an equivalent, one-dimensional one [2], [4]–[8]. Numerical methods have also been developed. For example, in [1] the parabolic variation is used. Maxwell's equations are solved both for the active layer and the confining layers, and then superposition is applied to both types of solutions to form a general expression for the field. These solutions and their derivatives are matched at the boundaries of the active layer, yielding an infinite system of linear homogeneous equations, whose solutions, numerically obtained, are the expansion coefficients for the mode in terms of the eigenfunctions of the active layer problem. Of course, direct numerical integration of the two-dimensional wave equation is possible, but the computation times are long compared to those required by the algorithm discussed in this paper.

For the type of variation considered here, a general field in the active layer must be expressed as a superposition of the few confined discrete modes plus an integral over the continuum. Leaky modes cannot be included in the expansion if the field is to decrease to zero for large distances from the stripe.

Direct application of the numerical method used in [1] results in a finite set of linear equations (due to the finite number of trapped modes) coupled with an integral equation (due to integral over the continuum). For the case in which only one trapped mode exists (the fundamental mode), an integral equation results, which can in principle be solved. However, these cases will be seen to correspond to structures with net modal loss or low gains very sensitive

Manuscript received May 6, 1982; revised June 22, 1982. This work was supported by the U.S. Army Research Office.

The authors are with the Department of Electrical Engineering, Southern Methodist University, Dallas, TX 75275.

0018-9480/82/1200-2139$00.75 ©1982 IEEE